A comparative assessment of information-exploitation techniques for GPR data inversion



2015 J. Phys.: Conf. Ser. 657 012010

(http://iopscience.iop.org/1742-6596/657/1/012010)

Journal of Physics: Conference Series **657** (2015) 012010 doi:10.1088/1742-6596/657/1/012010

# A comparative assessment of information-exploitation techniques for GPR data inversion

**M Salucci[1], L Tenuti[2], L Poli[2], G Oliveri[2] and A Massa[1,2]**
[1] ELEDIA Offshore Lab @ Paris, Laboratoire des Signaux et Systèmes (L2S, UMR CNRS 8506), 3 rue Joliot Curie, 91192 Gif-sur-Yvette, France
[2] ELEDIA Research Center, Department of Information Engineering and Computer Science, University of Trento, Via Sommarive 5, 38123 Trento, Italy
E-mail: andrea.massa@l2s.centralesupelec.fr

**Abstract.** The inversion of Ground Penetrating Radar (GPR) data requires the development of suitable information-exploitation techniques that are able to extract as much as possible information on the unknown targets from the available measurements. An innovative single-frequency (SF) inversion technique based on a deterministic conjugate-gradient (CG) minimization and the iterative multi-scaling approach (IMSA) is described. It is then shown how to improve the performances of the SF-IMSA-CG method by the introduction of an external frequency hopping (FH) iterative loop. On the one hand, the proposed FH-IMSA-CG method allows to exploit the intrinsic frequency diversity of wideband GPR measurements thanks to the FH strategy. On the other hand, the IMSA approach guarantees a significant reduction of the problem unknowns, providing an increased resolution within the identified regions of interest (RoIs). A numerical comparison shows the advantages of the FH-IMSA-CG over its single-frequency version. Moreover, the benefits of integrating the IMSA within the FH are verified by directly comparing the FH-IMSA-CG with its single-resolution (BARE) version (FH-BARE-CG).

## 1. Introduction

Ground penetrating radar (GPR) is one of the most widespread instrumentations for performing subsurface investigations in many fields of applications, ranging from civil engineering to archaeology [1]. Recently, an increasing amount of research has been focused on the development of fast, effective and robust algorithms for suitably processing the scattered radiation (i.e., the GPR radargram) and estimating the geometrical and dielectric characteristics of unknown objects embedded inside the inspected (inaccessible) domain. As a matter of fact, the reduced amount of collectable information due to the availability of aspect-limited measurements (i.e., often the antennas are placed only above the interface) and to the occurrence of non-negligible reflections in crossing heterogeneous media makes the retrieval of buried targets a quite challenging task. Following the above considerations, suitable information-exploitation techniques are needed to properly address the inversion of GPR data, both considering deterministic [2] and stochastic [3] approaches. When some *a-priori* information on the scenario at hand is available, such a task may be accomplished by introducing some mathematical approximations that allow to reduce the non-linearity of the problem (e.g., in the presence of weak scatterers [2, 4]). Similarly, compressive sensing (CS)-based techniques [4-6] have been proven to be very effective if the retrieved solution is sparse with respect to a properly chosen representation basis. Iterative multi-scaling approaches (such as, for example, the IMSA method [7]) can be successfully

employed to effectively tackle both the *non-linearity* and the *ill-posedness* of the subsurface inversion problem [2], leading to an increased resolution within the identified regions of interest (RoIs). Moreover, the intrinsic wideband nature of GPR data enables the use of techniques that are able to process different components of the measured spectrum, allowing to exploit the frequency-diversity as an additional source of information [5].

In this framework, this work presents an innovative imaging technique based on the integration of a deterministic conjugate-gradient (CG) method and the IMSA that is able to retrieve buried targets by processing a single-frequency (SF) component of the GPR spectrum. It is then shown how to enclose the SF-IMSA-CG method within an external frequency-hopping (FH) loop in order to exploit the additional information coming from multi-chromatic components of the data. A numerical assessment is given in order to verify the advantages of the FH-IMSA-CG method over the SF-IMSA-CG. Moreover, the benefits of integrating the IMSA within the FH are verified by directly comparing the FH-IMSA-CG with its single-resolution (BARE) version (FH-BARE-CG).

## 2. Mathematical formulation

Let be given a 2-D scenario where the investigation domain $D_{inv}$ is completely embedded inside a lossy homogeneous background with relative permittivity $\varepsilon_{rb}$ and conductivity $\sigma_b$ (Fig. 1).

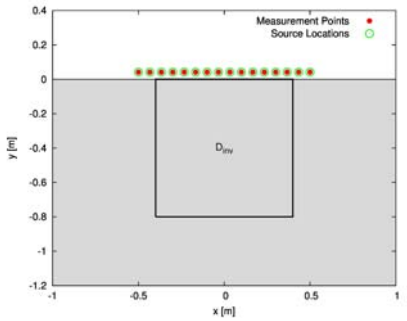


**Figure 1.** Geometry of the problem.

A set of $V$ $z$-directed ideal line sources are located in the upper half-space (free-space) at constant height $h$ above the interface ($y=0$) and are radiating a wide-band transverse-magnetic field $\mathbf{\Psi}^v_{inc}(\mathbf{r},t)=\Psi^v_{inc}(\mathbf{r},t)\hat{\mathbf{z}}$, $\mathbf{r}=(x,y)$ being the position vector. Moreover, let us assume that an unknown cylindrical scatterer with relative permittivity $\varepsilon_r(\mathbf{r})$ and conductivity $\sigma(\mathbf{r})$ is buried at a given depth inside $D_{inv}$. Under these hypothesis, the interactions between the $v$-th illumination and the lower half-space produce a total field $\mathbf{\Psi}^v_{tot}(\mathbf{r},t)=\left\{\Psi^v_{inc}(\mathbf{r},t)+\Psi^v_{scatt}(\mathbf{r},t)\right\}\hat{\mathbf{z}}$ that is collected by $M$ ideal field probes located above the interface at positions $\mathbf{r}^v_m$ ($m=1,...,M$, Fig. 1), $\Psi^v_{scatt}(\mathbf{r},t)$ being the time-domain field scattered by the buried target. By means of a Fast Fourier Transform (FFT) algorithm, the received radiation is transformed into the frequency domain, in which the scattering phenomena are completely modelled at a given frequency by means of the following set of non-linear equations

$$\begin{aligned} E^v_{scatt}(\mathbf{r}^v_m) &= k_b^2 \int_{D_{inv}} \tau(\mathbf{r}')E^v_{tot}(\mathbf{r}')G_{ext}(\mathbf{r}^v_m,\mathbf{r}')d\mathbf{r}' \\ E^v_{inc}(\mathbf{r}) &= E^v_{tot}(\mathbf{r}) - k_b^2 \int_{D_{inv}} \tau(\mathbf{r}')E^v_{tot}(\mathbf{r}')G_{\mathrm{int}}(\mathbf{r},\mathbf{r}')d\mathbf{r}' \end{aligned} \quad (1)$$

where $k_b$ is the wave-number in the lossy medium, $G_{ext}$ and $G_{\text{int}}$ are the external and internal Green's functions for the half-space, while $\tau(\mathbf{r})$ is the so-called contrast function and is defined as

$$\tau(\mathbf{r}) = \{\varepsilon_r(\mathbf{r}) - \varepsilon_{rb}\} + j\left\{\frac{\sigma_b - \sigma(\mathbf{r})}{2\pi f \varepsilon_0}\right\}. \tag{2}$$

The SF-IMSA-CG method extracts a single component of the transformed GPR spectrum and recovers an estimation of the unknown contrast and total field inside $D_{inv}$ in $S$ iterative steps. This method can be summarized as follows.

1. *Initialization*. At the first multi-scaling step ($s=1$) $D_{inv}$ is partitioned into $N$ square sub-domains ($N$ being the number of degrees-of-freedom of the scattered field [8]). The unknowns are initialized to the empty background [i.e., $\tau^{(0)}(\mathbf{r}_n) = 0.0$ and $E_{tot}^{v(0)}(\mathbf{r}_n) = E_{inc}^{v}(\mathbf{r}_n)$, for $n = 1,...,N$ and $v = 1,...,V$ ].
2. *Preliminary coarse reconstruction*. A CG deterministic approach is used to recover an initial low-resolution reconstruction by minimizing the following cost function

$$\Phi = \frac{\sum_{v=1}^{V}\sum_{m=1}^{M}\left|E_{scatt}^{v}(\mathbf{r}_m^v) - \widetilde{E}_{scatt}^{v}(\mathbf{r}_m^v)\right|^2}{\sum_{v=1}^{V}\sum_{m=1}^{M}\left|E_{scatt}^{v}(\mathbf{r}_m^v)\right|^2} + \frac{\sum_{v=1}^{V}\sum_{n=1}^{N}\left|E_{inc}^{v}(\mathbf{r}_n) - \widetilde{E}_{inc}^{v}(\mathbf{r}_n)\right|^2}{\sum_{v=1}^{V}\sum_{n=1}^{N}\left|E_{inc}^{v}(\mathbf{r}_n)\right|^2} \tag{3}$$

   where $\widetilde{E}_{scatt}^{v}(\mathbf{r}_m^v)$ and $\widetilde{E}_{inc}^{v}(\mathbf{r}_n)$ denote the computed scattered and incident field, respectively.
3. *Iterative multi-scaling loop*. At each $s$-th successive step ( $s = 2,...,S$ ), a clustering procedure [7] is applied to identify the RoI $D^{(s)}$ where the target has been localized at the previous step. An higher resolution image of $D^{(s)}$ is then obtained by means of the CG, by suitably mapping the solution found at the $(s-1)$-th step to properly initialize the problem unknowns.
4. *Termination*. The multi-scaling procedure is terminated when $s = S$ or when a suitable stopping criterion is met [7].

Given the intrinsic wide-band nature of GPR data, the performances of the SF-IMSA-CG can be improved by nesting it inside a FH external loop. The resulting FH-IMSA-CG method extracts $K$ frequency components of the measured spectrum inside the 3dB bandwidth of the radiated pulse (i.e., $f_{\min} \le f_1 \le ... \le f_K \le f_{\max}$ ). Then, each $k$-th frequency component is successively processed by means of the described algorithm in a cascaded fashion. At each frequency stage successive to the first one (i.e., $k = 2,...,K$ ), the solution found at the IMSA convergence step $S_{k-1}$ of the $(k-1)$-th stage is used to initialize the solution as follows

$$\begin{aligned} \tau_k^{(0)}(\mathbf{r}) &= \text{Re}\left\{\tau_{k-1}^{(S_{k-1})}(\mathbf{r})\right\} + j\frac{f_{k-1}}{f_k}\text{Im}\left\{\tau_{k-1}^{(S_{k-1})}(\mathbf{r})\right\} \\ E_{tot,k}^{(0)v}(\mathbf{r}) &= F\left\{\tau_k^{(0)}(\mathbf{r}); E_{inc,k}^{v}(\mathbf{r})\right\} \end{aligned} \tag{4}$$

where $F\{.\}$ indicates a 2-D method-of-moments (MoM) forward solver.

## 3. Numerical comparison

This section is aimed at assessing the potentialities, as well as the limits, of the proposed techniques when dealing with the reconstruction of unknown buried targets. In order to give a quantitative measure of the accuracy of the retrieved profiles, the same reconstruction errors defined in [9] are used

hereinafter. Moreover, in order to test the algorithms under realistic noisy conditions, the measured total field has been corrupted in time-domain by an additive zero-mean Gaussian noise $n^v\left(\mathbf{r}_m^v;t\right)$, by considering the following definition of signal-to-noise ratio

$$SNR = 10\log_{10}\sum_{v=1}^{V}\sum_{m=1}^{M}\int_{-\infty}^{+\infty}\left|\Psi_{tot}^v\left(\mathbf{r}_m^v;t\right)\right|^2 dt \Bigg/ \sum_{v=1}^{V}\sum_{m=1}^{M}\int_{-\infty}^{+\infty}\left|n^v\left(\mathbf{r}_m^v;t\right)\right|^2 dt \tag{5}$$

*3.1. Homogeneous scatterer at different depths*

In order to assess the effectiveness of the proposed inversion techniques, let us consider a square investigation domain of side 0.8 m (Fig. 1), with $\varepsilon_{rb} = 4.0$ and $\sigma_b = 10^{-3}$ S/m.

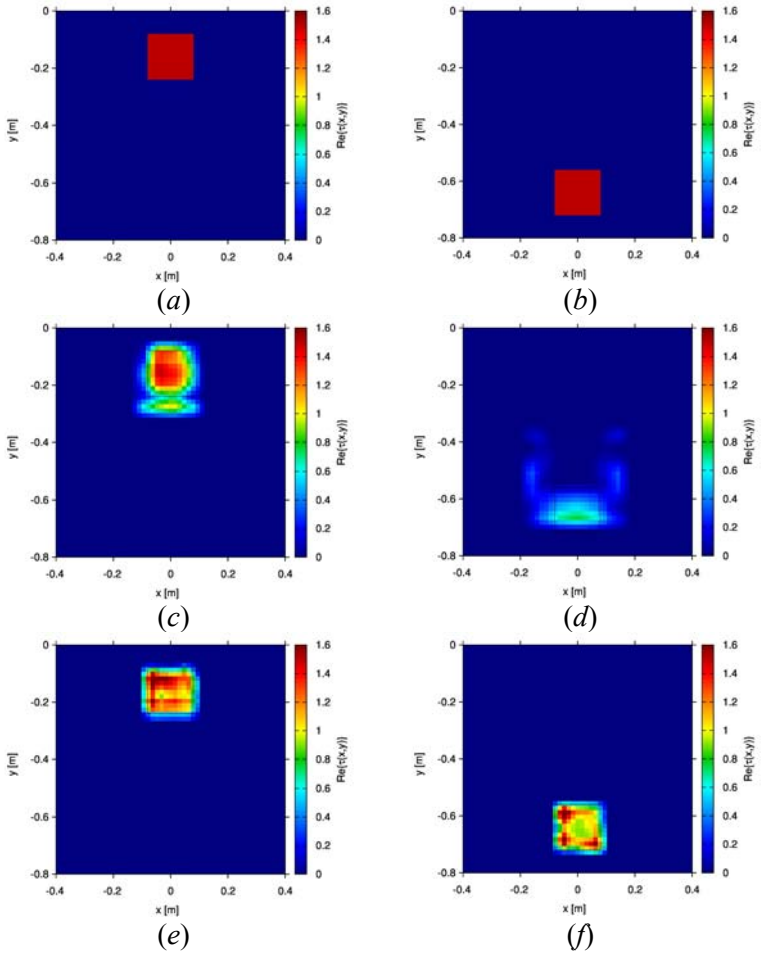


**Figure 2.** *Square scatterer at different depths* - (*a*)(*b*) Actual dielectric profiles and reconstructions by (*c*)(*d*) SF-IMSA-CG and (*e*)(*f*) FH-IMSA-CG, for *SNR* = 40 dB.

The synthetic field data have been generated by means of the GprMax2D simulator [10], by considering $V = 16$ sources equally spaced along a line of length 1 m located at $h = 0.04$ m above the interface. A Gaussian monocycle pulse with a central frequency of $f_0 = 300$ MHz and 3dB bandwidth covering the [200, 600] MHz range is used as excitation signal. For each illumination the scattered radiation is collected by a set of $M = 15$ probes co-located with the sources. This first analysis deals

with a benchmark square-shaped homogeneous scatterer ( $\tau = 1.5$ ) of side 0.16 m buried at different depths inside $D_{\text{inv}}$. More precisely, we suppose that the target barycentre is located at $(x_c, y_c) = (0.0, -0.16)$ m [Fig. 2(*a*)] and $(x_c, y_c) = (0.0, -0.64)$ m [Fig. 2(*b*)], respectively. The retrieved profiles by the SF-IMSA-CG are shown in Figs. 2(*c*)-2(*d*), when considering a single frequency component corresponding to $f_0$ and $SNR = 40$ dB. As it can be easily noticed, the quality of the reconstructions significantly degrades as the depth of the target is increased [Fig. 2(*c*) vs. Fig. 2(*d*)]. Such a consideration is confirmed by the computed internal error [i.e., $\Xi_{\text{int}}^{SF-IMSA-CG} = 1.74 \times 10^{-1}$ for Fig. 2(*c*) and $\Xi_{\text{int}}^{SF-IMSA-CG} = 4.21 \times 10^{-1}$ for Fig. 2(*d*)].

On the other hand, Figs. 2(*e*)-2(*f*) show the reconstructions obtained by the FH-IMSA-CG approach, considering $K = 5$ equally-spaced frequency components within the [200, 600] MHz bandwidth. As expected, a non-negligible improvement in terms of reconstruction accuracy is observed with respect to the SF approach, thanks to the exploitation of the additional information coming from multi-frequency GPR data. The advantage of using the FH strategy becomes relevant when dealing with the retrieval of the deepest object [Fig. 2(*f*) vs. Fig. 2(*d*)]. In this case, the FH-IMSA-CG is able to provide a better reconstruction of the object shape, as well as of its dielectric characteristics, as denoted by a significantly lower internal error ( $\Xi_{\text{int}}^{FH-IMSA-CG} = 2.21 \times 10^{-1}$ ).

*3.2. Inhomogeneous scatterer*

The next numerical benchmark considers an inhomogeneous scatterer [Fig. 3(*a*)] characterized by an inner core with $\tau_{\text{int}} = 2.0$ surrounded by an external region with $\tau_{ext} = 1.0$.

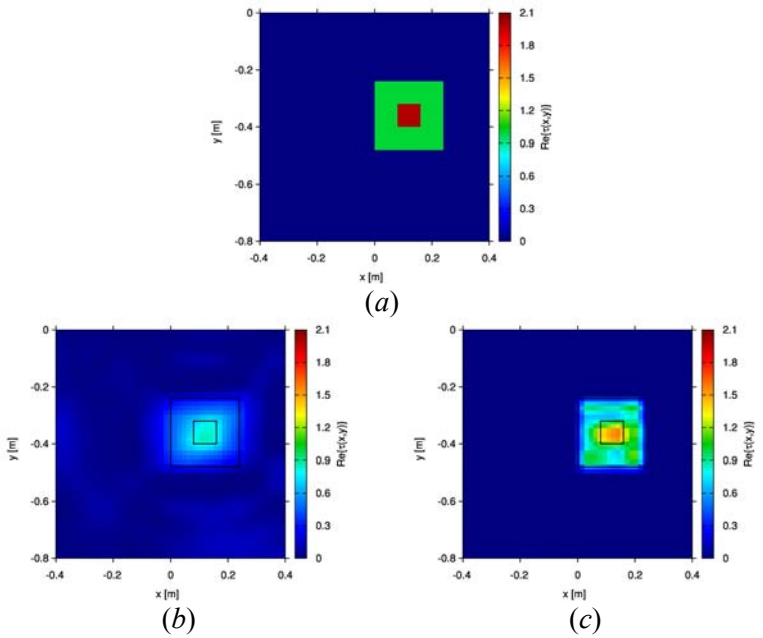


**Figure 3.** *Inhomogeneous scatterer* - (*a*) Actual dielectric profile and retrieved profiles by (*b*) FH-BARE-CG and (*c*) FH-IMSA-CG for *SNR* = 50 dB.

All the parameters are the same of the previous analysis, except from the number of sources and measurement points, which has been set to $V = 20$ and $M = 19$, respectively. The retrieved profiles for both the single-resolution FH-BARE-CG [Fig. 3(*b*)] and the multi-resolution FH-IMSA-CG [Fig. 3(*c*)] are shown in Fig. 3, when $SNR = 50$ dB. As it can be observed, the FH-IMSA-CG is not only able to suppress the undesired artefacts in the background region, but it also improves the overall

quality of the reconstruction, by correctly identifying the presence of an higher contrast within the inner core of the target, as further confirmed by the reconstruction error [$\Xi_{tot}^{FH-IMSA-CG} = 1.62 \times 10^{-2}$ for Fig. 3(*c*) vs. $\Xi_{\text{int}}^{FH-BARE-CG} = 7.53 \times 10^{-2}$ for Fig. 3(*b*)]. Thanks to a reduced number of unknowns, a remarkable improvement is observable also when considering the computational costs (i.e., $\Delta t^{FH-IMSA-CG} \approx 2.5 \times 10^4$ s vs. $\Delta t^{FH-BARE-CG} \approx 7.0 \times 10^4$ s on a standard laptop with 4 GB of RAM memory).

## 4. Conclusions

A comparative assessment between different information-exploitation techniques for the inversion of GPR data has been presented. It has been shown that the proposed FH-IMSA-CG method is able to overcome, in terms of reconstruction accuracy, the SF-IMSA-CG method thanks to its ability to exploit the additional information coming from multiple frequency components of the measured GPR spectrum. The advantages of the FH-IMSA-CG over its single-resolution version (FH-BARE-CG) have been also proved by means of a representative numerical example. The use of the IMSA approach has allowed a significant reduction of the problem unknowns, providing an increased resolution within the identified RoIs. Moreover, a remarkable improvement in terms of computational times has been obtained.

## References

[1] Leckebusch J 2003 Ground-penetrating radar: a modern three-dimensional prospection method *Archaeological Prospection* **10** 213-240

[2] Salucci M, Sartori D, Anselmi N, Randazzo A, Oliveri G and Massa A 2013 Imaging buried objects within the second-order Born approximation through a multiresolution-regularized inexact-Newton method *Int. Symp. Electromag. Theory (Hiroshima, Japan)* 116-118

[3] Rocca P, Benedetti M, Donelli M, Franceschini D and Massa A 2009 Evolutionary optimization as applied to inverse problems *Inverse Problems* **25** 1-41

[4] Oliveri G, Anselmi N and Massa A 2014 Compressive sensing imaging of non-sparse 2D scatterers by a total-variation approach within the Born approximation *IEEE Trans. Antennas Propag.* **62** 5157-5170

[5] Poli L, Oliveri G, Ding P-P, Moriyama T and Massa A 2014 Multifrequency Bayesian compressive sensing methods for microwave imaging *J. Opt. Soc. Am.* A **31** 2415-2428

[6] Poli L, Oliveri G and Massa A 2013 Imaging sparse metallic cylinders through a local shape function Bayesian compressive sensing approach *J. Opt. Soc. Am.* A **30** 1261-1272

[7] Caorsi S, Donelli M, Franceschini D and Massa A 2003 A new methodology based on an iterative multiscaling for microwave imaging *IEEE Trans. Microwave Theory Tech.* **51** 1162-1173

[8] Bucci O M, Crocco L, Isernia T and Pascazio V 2001 Subsurface inverse scattering problems: quantifying qualifying and achieving the available information *IEEE Trans. Geosci. Remote Sensing* **39** 2527-2538

[9] Moriyama T, Salucci M, Oliveri G, Tenuti L, Rocca P and Massa A 2014 A Multi-scaling deterministic imaging for GPR survey *Proc. 2014 IEEE Antenna Conf. Ant. Meas. Appl. (Antibes Juan-les-Pins)* 1-3

[10] Giannopoulos A 2005 Modelling ground penetrating radar by GprMax *Construct. Build. Mater.* **19** 755 -762

## Acknowledgment

This work has been partially supported by the SIRENA project (2014-2017) funded by DIGITEO (France) under the "Call for Chairs 2014" and benefited from the networking activities carried out within the EU funded COST Action TU1208 "Civil Engineering Applications of Ground Penetrating Radar".